energies

MDPI

Article

Flat Unglazed Transpired Solar Collector: Performance Probability Prediction Approach Using Monte Carlo Simulation Technique

Sajna Parimita Panigrahi [1], Sarat Kumar Maharana [2], Thejaraju Rajashekaraiah [1], Ravichandran Gopalashetty [1], Mohsen Sharifpur [3,4,*], Mohammad Hossein Ahmadi [5,*], C. Ahamed Saleel [6] and Mohamed Abbas [7,8]

1 Department of Mechanical and Automobile Engineering, School of Engineering and Technology, CHRIST (Deemed to Be University), Bangalore 560029, Karnataka, India
2 Department of Aeronautical Engineering, Acharya Institute of Technology, Bangalore 560107, Karnataka, India
3 Department of Mechanical and Aeronautical Engineering, University of Pretoria, Hatfield 0028, South Africa
4 Department of Medical Research, China Medical University Hospital, China Medical University, Taichung 404327, Taiwan
5 Faculty of Mechanical Engineering, Shahrood University of Technology, Shahrood 3619995161, Iran
6 Department of Mechanical Engineering, College of Engineering, King Khalid University, P.O. Box 394, Abha 61421, Saudi Arabia
7 Electrical Engineering Department, College of Engineering, King Khalid University, P.O. Box 394, Abha 61421, Saudi Arabia
8 Electronics and Communications Department, College of Engineering, Delta University for Science and Technology, Gamasa 35712, Egypt
* Correspondence: mohsen.sharifpur@up.ac.za (M.S.); mohammadhosein.ahmadi@gmail.com or mhosein.ahmadi@shahroodut.ac.ir (M.H.A.)

check for updates

Citation: Parimita Panigrahi, S.; Kumar Maharana, S.; Rajashekaraiah, T.; Gopalashetty, R.; Sharifpur, M.; Ahmadi, M.H.; Saleel, C.A.; Abbas, M. Flat Unglazed Transpired Solar Collector: Performance Probability Prediction Approach Using Monte Carlo Simulation Technique. *Energies* **2022**, *15*, 8843. https://doi.org/10.3390/en15238843

Academic Editor: Tapas Mallick

Received: 23 September 2022
Accepted: 11 November 2022
Published: 23 November 2022

Publisher's Note: MDPI stays neutral with regard to jurisdictional claims in published maps and institutional affiliations.

Abstract: Engineering applications including food processing, wastewater treatment, home heating, commercial heating, and institutional heating successfully use unglazed transpired solar collectors (UTCs). Trapping of solar energy is the prime goal of developing an unglazed transpired solar collector. The UTC is usually developed in and around the walls of the building and absorbs the solar energy to heat the air. One of the key challenges faced by the UTC designer is the prediction of performance and its warranty under uncertain operating conditions of flow variables. Some of the flow features are the velocity distribution, plate temperature, exit temperature and perforation location. The objective of the present study was to establish correlations among these flow features and demonstrate a method of predicting the performance of the UTC. Hence, a correlation matrix was generated from the dataset prepared after solving the airflow over a perforated flat UTC. Further, both strong and weak correlations of flow features were captured through Pearson's correlation coefficient. A comparison between the outcomes from a linear regression model and that of computational simulation was showcased. The performance probability for the UTC was interlinked with correlation matrix data. The Monte Carlo simulation was used to predict the performance from random values of the flow parameters. The study showed that the difference between the free stream value of temperature and the value of temperature inside the UTC's chamber varied between 15 and 20 °C. The probability of achieving system efficiency greater than 35% was 55.2%. This has raised the hope of recommending the UTC for drying and heating where the required temperature differential is within 20 °C.

Keywords: solar energy; Monte Carlo simulation; unglazed transpired solar collector (UTC); probability prediction

1. Introduction

Engineering applications including food processing, wastewater treatment, home heating, commercial heating, and institutional heating successfully use unglazed transpired

solar collectors (UTCs). By passing through perforated cladding inside the residential environment, the surrounding air is preheated by the solar collector. Since corrugated UTCs [1–4] are said to be more efficient than the flat type, solar photovoltaic cells are also integrated into the system to provide both power and heat. UTCs are typically used to produce the thermal buoyancy effect, and perforated UTCs are used to create important phenomena such as separation, reattachment, and impingement. When travelling from a perforated section to a flat region, the flow regime changes from laminar to turbulent. Non-homogeneity suction is caused by smaller perforated region features that create a local turbulent flow regime. Some investigations on the perforation spacing, suction flow and velocity field over plate-type UTCs have been carried out by early researchers. Findings from thermodynamic analysis [5], heat transfer analysis and evaluation [6–9], and computational fluid dynamics of flow over UTCs [10] have been reported. To complement the findings on UTCs, both numerical and experimental investigations [11–15] were carried out. Most of these studies were on heat and air flow analysis of photovoltaic thermal systems [16–22]. Thermal modeling and parametric studies to understand the performance of UTCs [23–28] were never easy for early researchers because of challenges posed by the uncertain conditions of incoming airflow [29–31] over a perforated UTC. The performance prediction of the solar energy [32–35] when the system is in use [36–41] is a major challenge under varying conditions of airflow and other key parameters of the UTC.

The performance probability of a flat UTC needs to be studied properly because the UTC is anticipated to function under a great deal of uncertainty when it is put into operation. The constant performance of a UTC in use would be significantly impacted by the substantial fluctuations and dispersion of a few key flow elements.

Investigating the factors for improved performance is a wonderful idea to determine whether a UTC is acceptable. Since the operating conditions of air entering a UTC are usually unknown, an uncertainty analysis was also proposed to understand the performance probability of the UTC. The flow features employed in the computation of UTC performance were compiled into a correlation matrix. For correlation, it is necessary to have a dataset of flow features that have been created by separately solving flows over an unglazed transpired solar collector (UTC), which is intended to gather heat from an outside source.

The present study attempted to establish the correlations between plate temperature, exit temperature, the velocity distribution in the chamber and the location of the UTC perforations. The direct Monte Carlo simulation technique was ideal for achieving the study's objectives. We sought to predict the performance probability of a UTC in this paper because, to our knowledge, no earlier reports of such attempts have been published. The objective was to compute the likelihood (or probability) of accepting UTC performance when uncertain situations arise during its operation. The performance probability computation was a necessity because, in real-world applications of wind flow and solar energy, many uncertain parameters and their values affect the potential performance of a UTC.

2. Methodology

2.1. Modelling

The cornerstone of the analysis in this study was a set of fundamental governing equations of fluid dynamics—the continuity, momentum and energy equations [42], which are presented as Equations (1)–(4), respectively, below.

Continuity equation:

$$\frac{\partial \rho}{\partial t} + \nabla.(\rho \vec{v}) = 0 \quad (1)$$

Momentum equation:

$$\frac{\partial (\rho \vec{v})}{\partial t} + \nabla.(\rho \vec{v} \vec{v}) = -\nabla p + \nabla.(\bar{\bar{\tau}}) + \rho \vec{g} + \vec{F} \quad (2)$$

where is p the static pressure, $\overline{\overline{\tau}}$ is the stress tensor, $\rho\vec{g}$ and $\vec{F}$ are the gravitational body force and external body forces, respectively.

The stress tensor $\overline{\overline{\tau}}$ is given below.

$$\overline{\overline{\tau}} = \mu\left[(\nabla\vec{v} + \nabla\vec{v}^{T}) - \frac{2}{3}\nabla.\vec{v}\ I\right] \quad (3)$$

where μ is the molecular viscosity, I is the unit tensor, and the second term on the right hand is the effect of volume dilation.

Energy equation:

$$\rho C_p\left[\frac{\partial T}{\partial t} + (\vec{v}\ .\ \nabla)T\right] = k\nabla^2 T + \varnothing \quad (4)$$

where C_p is the specific heat, T is the temperature, k is the thermal conductivity of the fluid, and $\varnothing$ represents dissipation.

For the closure of the unknown Reynolds stress terms (components of total stress tensor) and to model the turbulence effect in the flow, the turbulence models [42] were appropriately chosen for the computational modeling of the flow over the UTC.

The computational domain used in the study is shown in Figure 1a. An area of 0.6 m × 0.6 m with a cavity height of 0.15 m was chosen for the UTC plate. A 1.59 mm diameter perforation was developed for a pitch of 16.89 mm with a wall thickness of 0.86 mm. The upper part of the domain was developed for a height of 0.3 m to accommodate the boundary layer thickness. Details on boundary conditions used for the simulation are mentioned in Table 1. The pattern and orientation of the perforations on the plate (zx-plane) are displayed in Figure 1b. Basically, surface-2 (with perforations) is a wall with heat flux = 600 W/m^2 and acts as an inlet (where suction velocity is defined) to the cavity just below it.

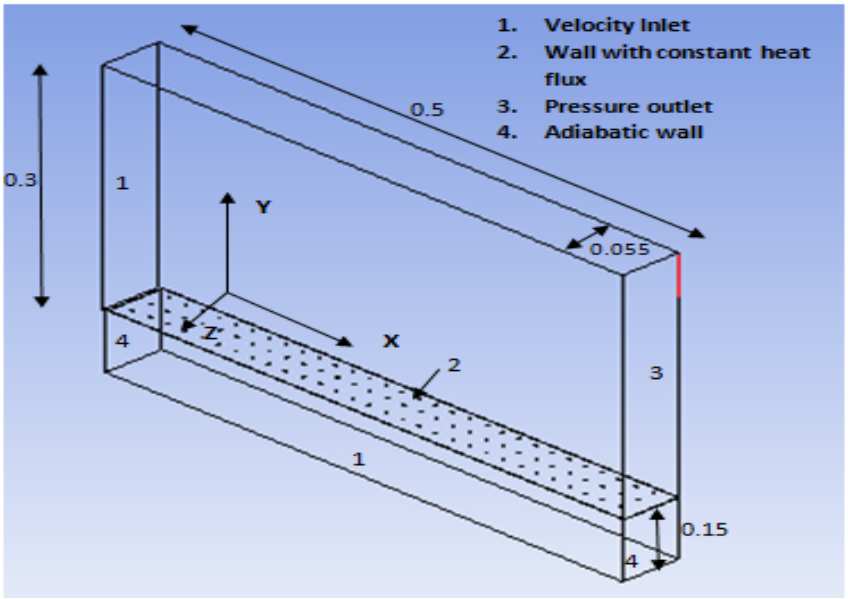

(**a**)

Figure 1. *Cont.*

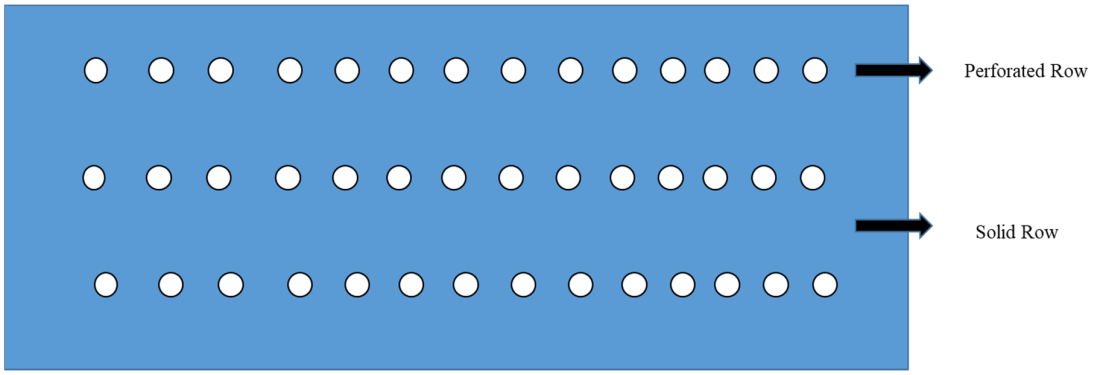

(**b**)

Figure 1. (**a**) Flat UTC model configuration (unit: m)—Computational domain; (**b**) model of perforated and solid rows arrangement.

Table 1. Details of Boundary States.

Surface Number	Boundary Condition Type	Flow Variable
1	Inflow	Flow enters at 1% turbulence with 1 m/s speed at 298 K
2	Wall	Solar heat flux over wall = 600 W/m^2
3	Outflow	Open to the atmospheric pressure
4	Wall	Insulated wall

A semi-implicit method for pressure-linked equations (SIMPLE) algorithm, an iterative method, was selected in the CFD solver—Ansys® Fluent 20.0, to achieve the solutions of the primitive flow variables. The inflow velocity, u, along surface-1 (indicated as 1 in the domain) varied from 0 to 1 m/s. The direction of this velocity was from left to right of the domain. The suction velocity, v = V_s (emanating from surface-2) in the cavity, varied from 0.045 to 0.077 m/s, and its direction was vertically downward. All of the boundary conditions are shown in a schematic diagram in Figure 2. The values were decided based on the prevailing experimental conditions and studies in the literature [1,2].

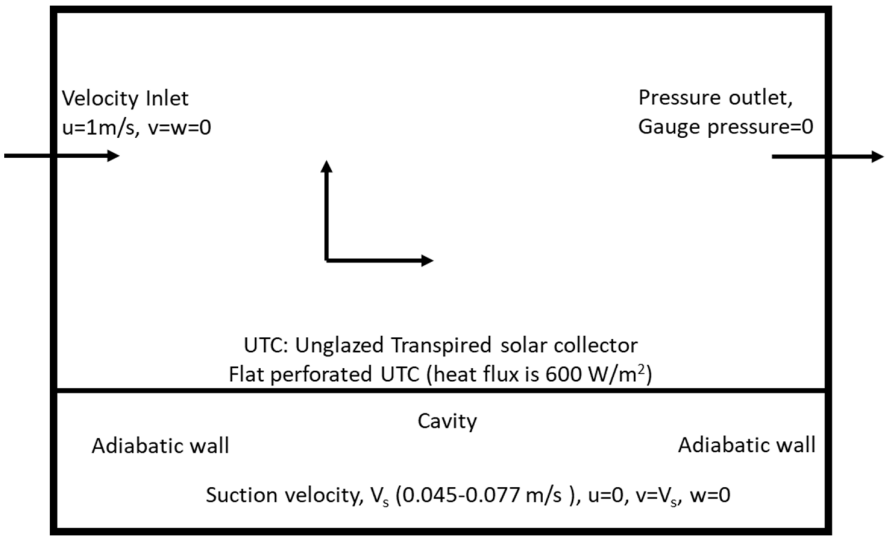

Figure 2. Schematic diagram of boundary conditions for the flow domain in the *xy* plane.

2.2. Mesh Development Analysis

The residuals were calculated under the same boundary conditions with an absolute tolerance value of 10^{-6} for all variables of flow. A grid independence check was performed

at 0.286 million, 0.2 million, and 0.135 million of grid points for the same computational domain. The mesh analysis was carried out for three different mesh sizes (in each case study), and their values are displayed in Table 2. The plate temperature reported for inlet velocity of 1 m/s (using numerical method) and that noted for the same inlet velocity (using experimental method) differed by 3% only. A similar observation (less than 5% difference) was made for the plate temperature for the inlet velocities of 0.077 and 0.045 m/s for the mesh sizes mentioned below.

Table 2. Mesh Analysis.

Plate Temperature (K)	Wind Speed and Suction Velocity	Mesh Size			Experimental Data
		Mesh 1	Mesh 2	Mesh 3	
Case Study 1	1 m/s & 0.077 m/s	314/305.9	314.5/305.7	314.7/305.0	313.9/306.5
Case Study 2	1 m/s & 0.045 m/s	315.4/307	314.8/307.1	313.7/306.9	313.9/306.5

3. Results and Discussion

Simulation and experimental results were validated for the case studies as mentioned in Table 2. Figure 3a displays the plate temperature, and Figure 3b shows cavity exit air temperature for laminar and turbulent flows using standard k-epsilon (k-ε) and shear stress transport (SST) k-omega (k-ω) turbulence models. The Eulerian model for CFD simulation was applied in this study.

In the present study, the intent was to understand the mean flow characteristics under turbulent flow conditions, and hence, k-epsilon [42], a two-equation model, was used. To understand the transport of shear stress (indicated in the stress tensor of the momentum equation), the SST k-ω model was introduced for closure of the solution. A comparison of numerical results and their validation with experimental data are shown in Figure 3a,b.

The values of temperature obtained using the experimental method and numerical technique compared fairly well. The standard k-epsilon model predicted values of plate temperature in a manner consistent with the experimental values. The predictions of values of temperatures (both plate and cavity exit air temperatures) by laminar flow simulations and turbulent flows (using the above-mentioned turbulence models) were quite complementary in terms of the trends and matched with their corresponding experimental values [1]. The prediction of the y-component of velocity along the flow domain is shown in Figure 3c. The figure shows a scale bar that indicates the maximum and minimum values of mean U_y. It was computed by using the SST k-ω turbulence model. The model had better superiority and relevance in predicting the profile of the velocity component. The reason for this decision was that prediction of the velocity component is linked to the transport of shear stress and hence the rate-of-change of deformation of a fluid in an enclosed cavity. The k-ε model could also be used to perform the same prediction in this case.

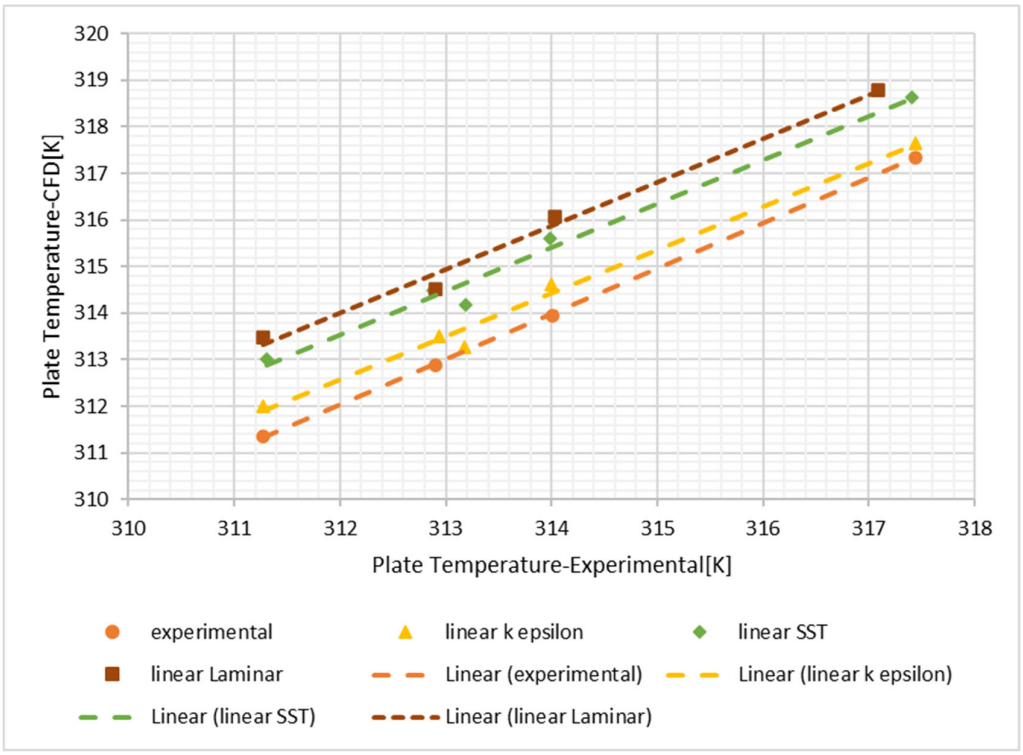

(**a**)

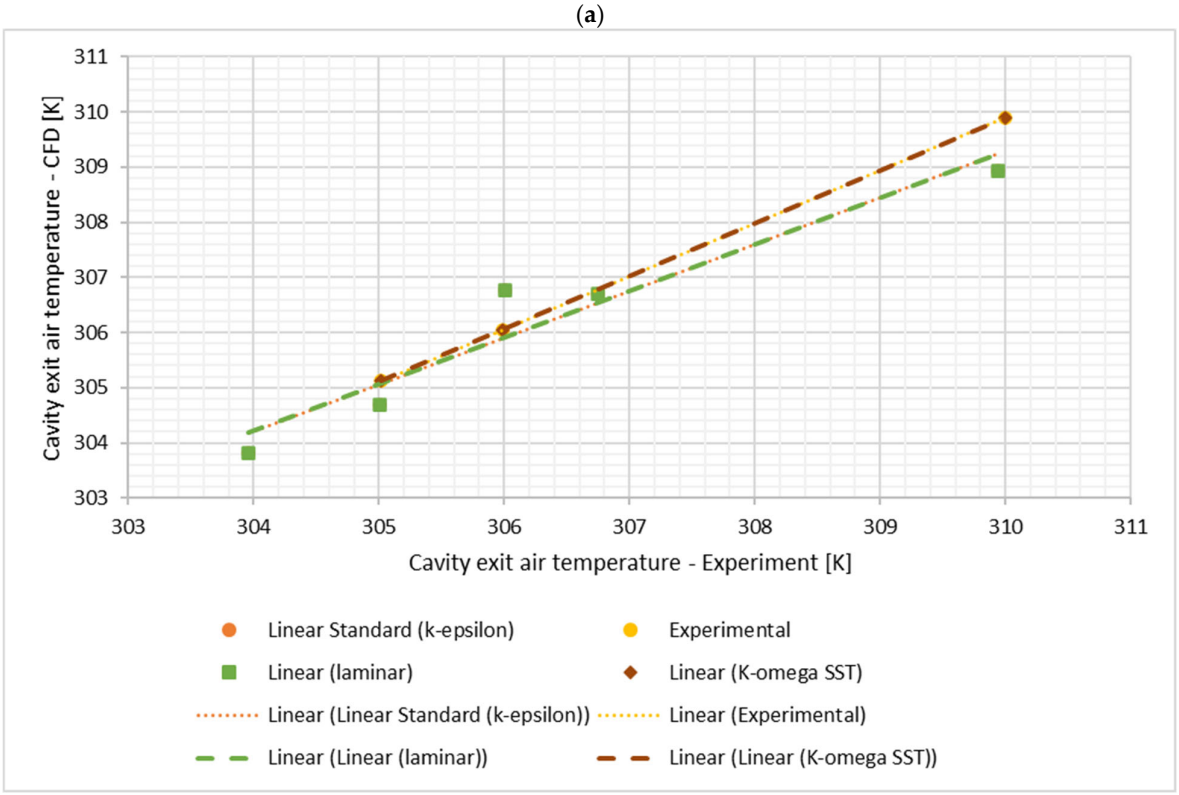

(**b**)

Figure 3. *Cont.*

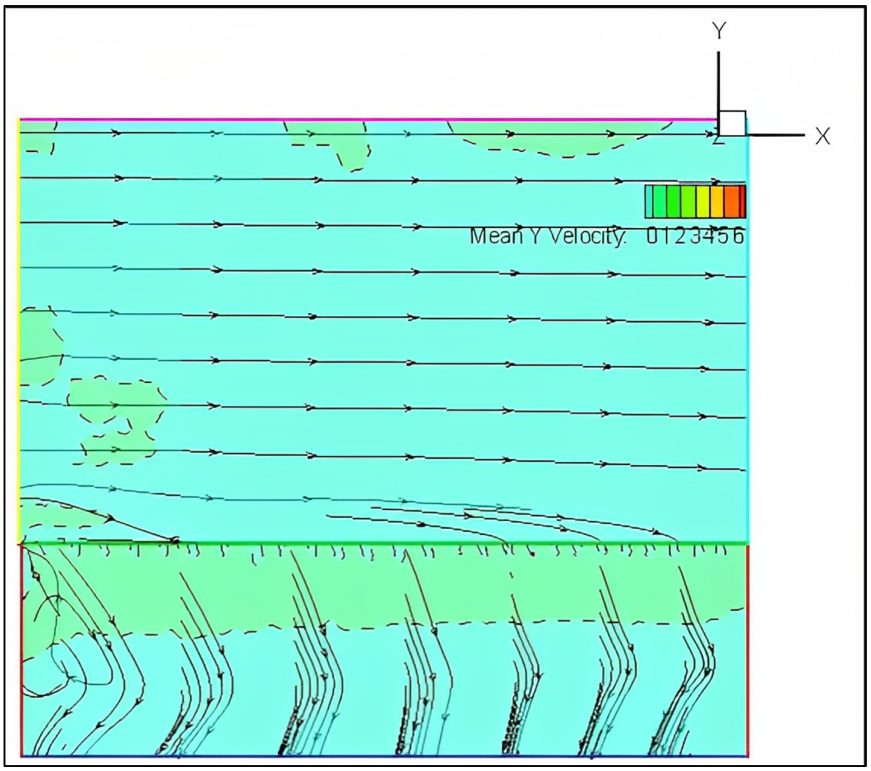

(**c**)

Figure 3. Comparison of CFD results and experimental data [1] for flat UTC model: (**a**) Plate surface temperature [K]); (**b**) Cavity exit air temperature [K]); (**c**) CFD Model analysis of Cavity.

Figure 4a shows a comparison of the vertical velocity (U_y) profile of air inside the chamber receiving a suction velocity V_s = 0.077 m/s. A higher value of U_y was predicted in the profile with the laminar model as compared to the two turbulent models (k-ε and SST k-ω models). Between Y = 0.21 and 0.31 (middle of the cavity) the predicted U_y rose sharply and remained at almost the same value. The non-dimensional quantity U_y/U_∞ is shown on the horizontal axis where U_∞ is the freestream velocity of air, and Y, the vertical distance from the base of chamber, is shown on the vertical axis. From Y = 0.31 to 0.51, the value of U_y rose. This change was due to the inherent nature of the flow near the walls where friction deterred the growth of velocity (and had no slip condition), and near the surface of the UTC (perforated one), the speed was hugely affected by the suction velocity and hence aided in increasing the magnitude of U_y.

The three CFD models' predictions of plate temperature are shown in Figure 4b for Y = 0.31 to 0.5 for the suction velocity of 0.077 m/s. The maximum plate temperature was predicted by the laminar model, and the minimum was obtained through the k-ε model. The range of temperature predicted by each CFD model is displayed through a box plot in Figure 4c. To find the best fit line for the differently predicted temperature values with respect to location, a simple regression analysis was performed, and the results are presented in Figure 4d for the exit temperature and in Figure 4e for the plate temperature. The model fit well and linearly for exit temperature, whereas the non-linearity effect was seen in plate temperature.

Basically, the plots shown in the Figures 4d,e and 5a–e are the results of linear regression between the response and predictor variables. So, the regression line or the best fit line (predicted by the regression method) passed through the actual data points.

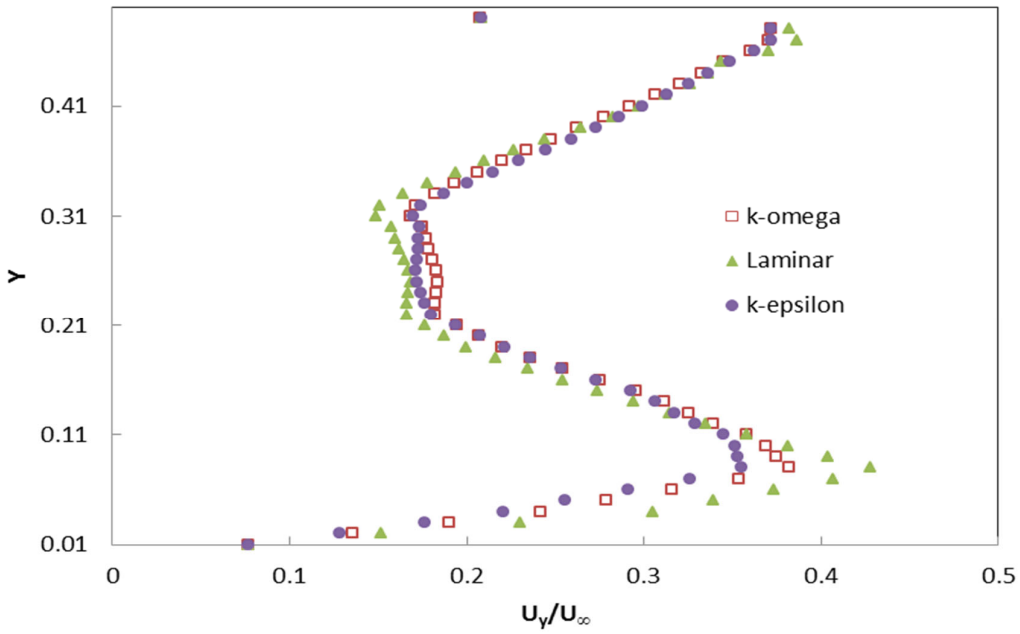

(**a**)

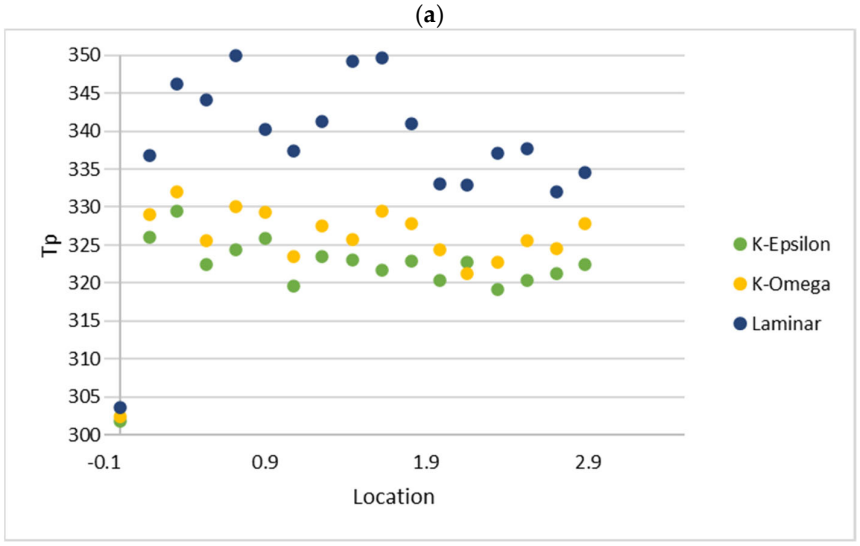

(**b**)

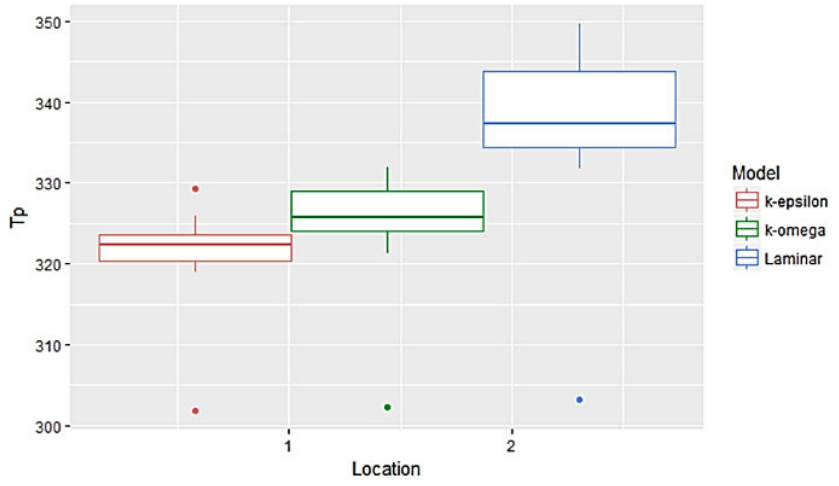

(**c**)

Figure 4. *Cont.*

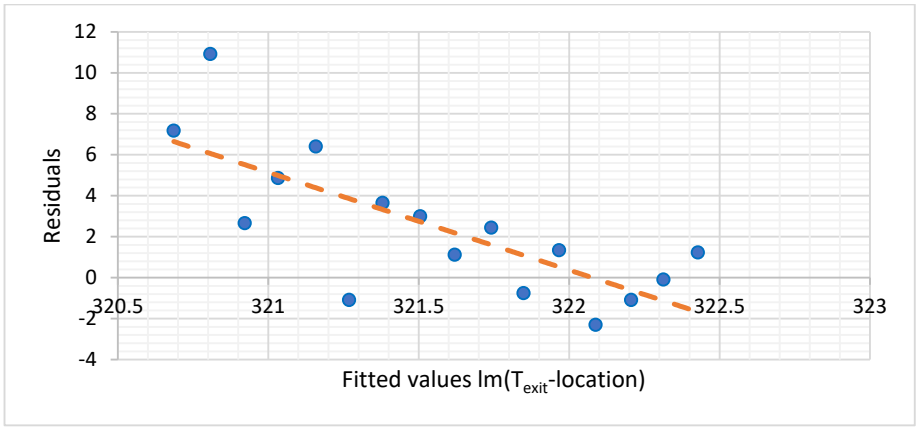

(**d**)

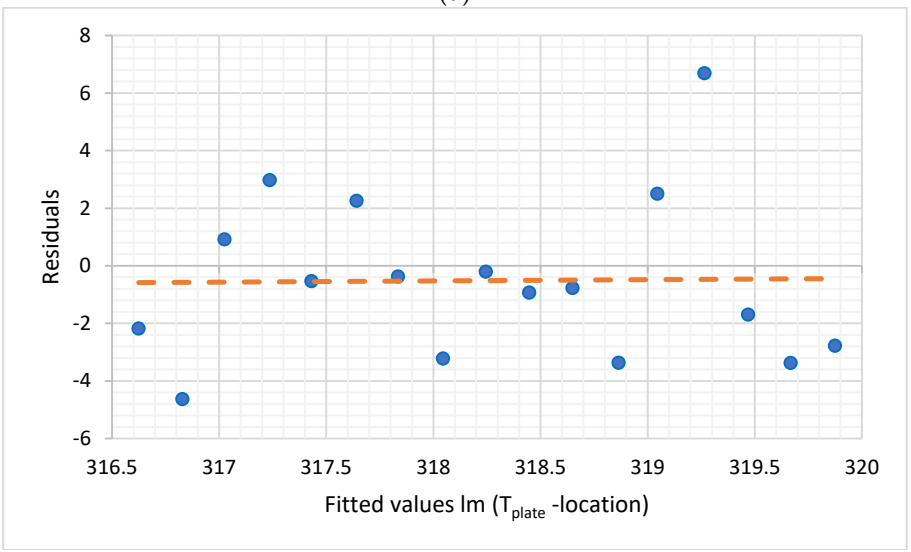

(**e**)

Figure 4. (**a**) Comparison of velocity profile U_y of hot air within the chamber predicted by 3 different CFD models for suction velocity, Vs = 0.077 m/s. (**b**) Comparison of plate temperature predicted by 3 different CFD models for suction velocity, Vs = 0.077 m/s. (**c**) Box plots show the range and characteristics of plate temperature predicted by 3 different CFD models for suction velocity, Vs = 0.077 m/s. (**d**) Scatter plot for the distribution of exit temperature T_{exit} (fitted value) versus location. (**e**) Scatter plot for the distribution of plate temperature (fitted value) versus location.

The exit temperature (T_{exit}) and location of perforations (measured from the domain's inlet) are shown in Figure 4d with a difference; higher temperatures were recorded further from the inlet. The best fit line passed through the actual data points. Residuals between the regression line and the actual distribution of data points decreased over the position of perforation. A similar observation was made for plate temperature in Figure 4e. However, the regression line and actual data distribution trend were unpredictable in this case, and hence, a wider variation in plate temperature (T_{plate}) was not visible in the plot. The lm () function of the R language (an open-source programming language) was used to carry out regression.

Figure 5a displays the plot between residuals and fitted value over location; for the residual = 0, the fitted values were not well behaved and followed a non-linear relationship. Figure 5b displays the plot between residuals and fitted value over exit temperature; the relationship also displayed a non-linear behavior for residual value = 0 for velocity in the *y*-direction. Figure 5c is a residual versus fitted plot. Around the residual value = 0, the fitted values were very close to the regression line, and the response (T_e) from the system

met the regression line (residual is zero); hence, a linear relationship was observed between T_e and the location of the hole.

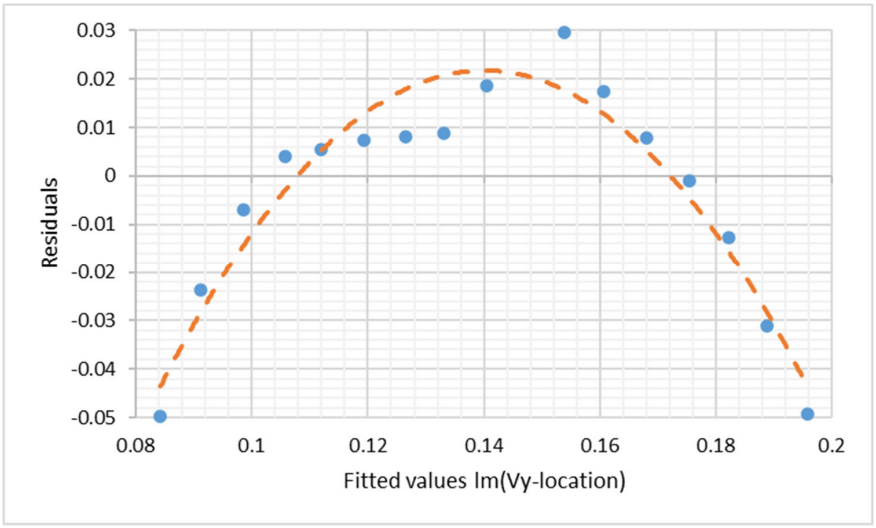

(**a**)

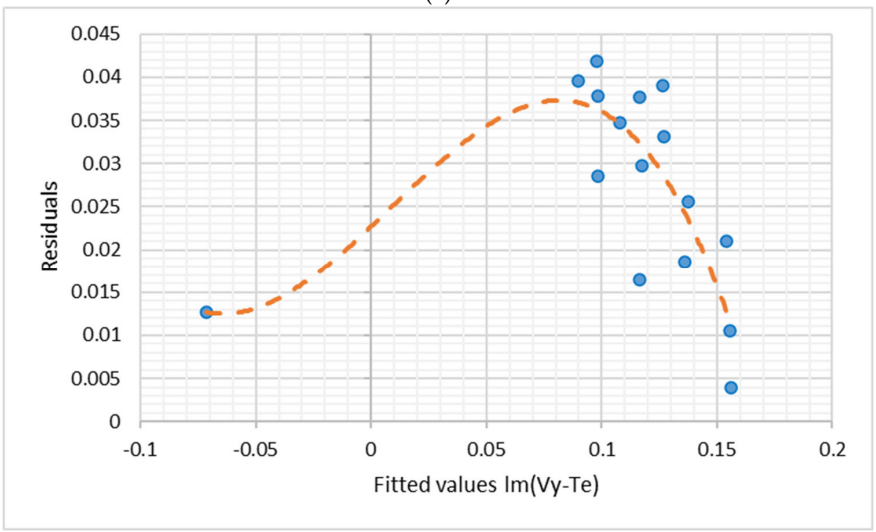

(**b**)

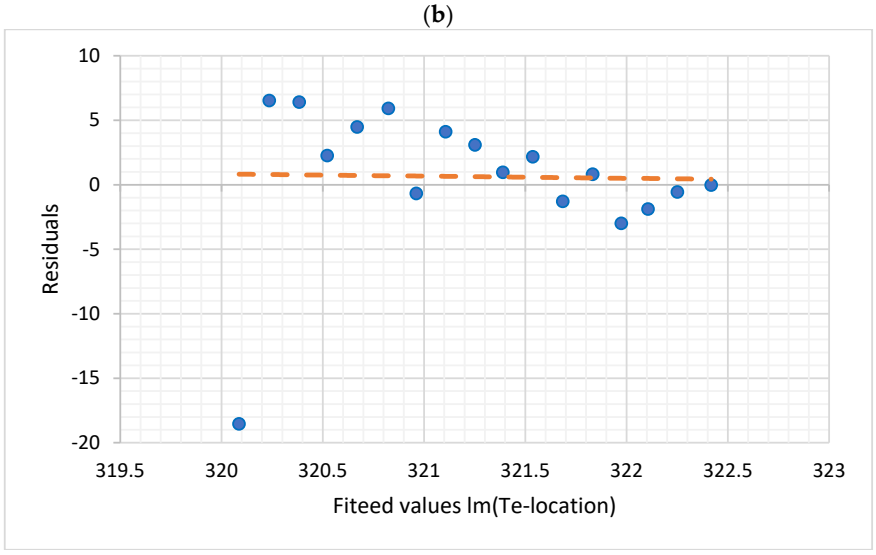

(**c**)

Figure 5. *Cont.*

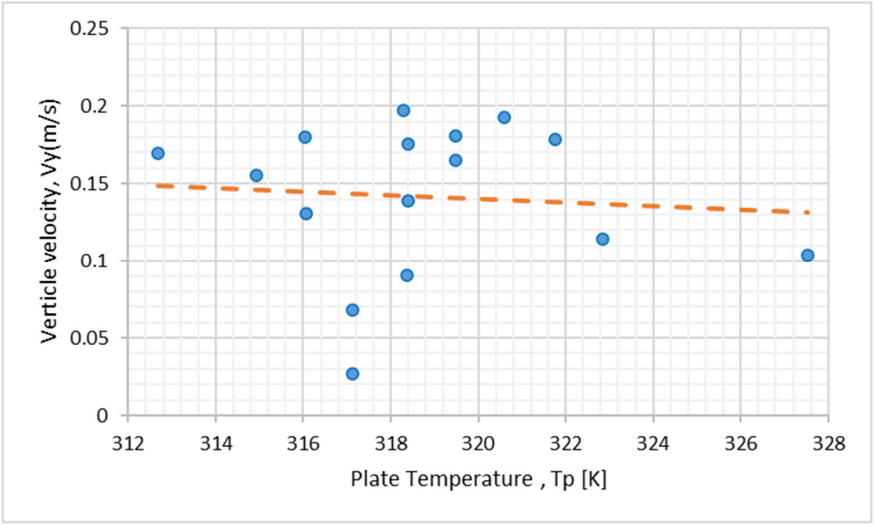

(**d**)

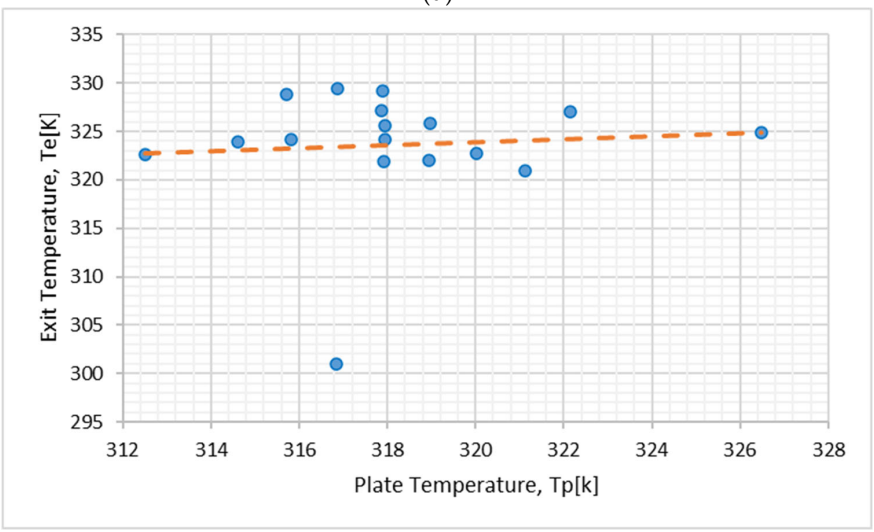

(**e**)

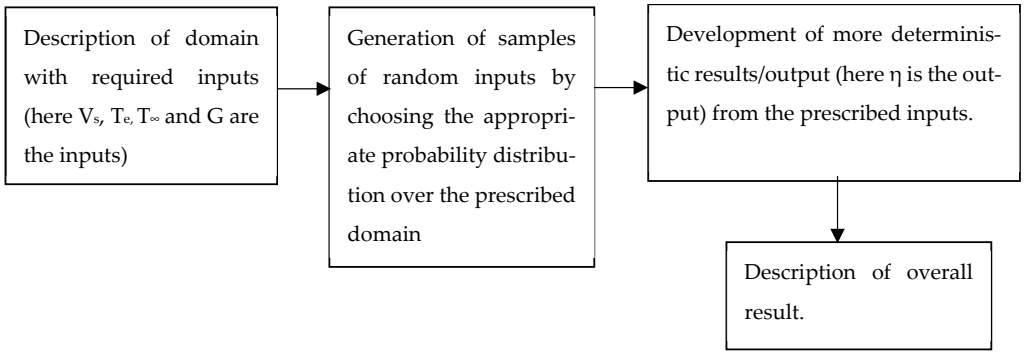

(**f**)

Figure 5. (**a**) Scatter plot for the distribution of mean Y-velocity (fitted value) versus location. (**b**) Scatter plot of Y-velocity of T_{exit} versus residuals. (**c**) Scatter plot of T_{exit} location versus residuals. (**d**) Cavity vertical velocity versus plate temperature with regression line. (**e**) Exit temperature versus plate temperature with regression line. (**f**) Flow diagram of Monte Carlo technique.

The variation in plate temperature and exit temperature over the y-component velocity is displayed in Figure 5d,e. The regression line determined for the values was slightly linear and the equal error variance was reasonable in this case. The correlation matrix shown in

Table 3 displays the coefficient of correlation, a statistic to measure the linear relationship between any two variables. The variables selected from the study were exit temperature (T_e), vertical velocity (V_y), experimental exit temperature (T_{ee}), numerical plate temperature (T_p) and experimental plate temperature (T_{pe}). One of the most common ways of measuring a linear correlation between two variables is Pearson's correlation coefficient [43]. It is the correlation statistic that measures the statistical strength, which varies from −1 to +1, between two continuous variables. The formula for r is given below in Equation (5). In the formula given below, r_{xy} represents the correlation coefficient between the two variables x and y, n is the number of observations, x_i is the value of the ith observation of x, and y_i is the value of the ith observation of y.

$$r_{xy} = \frac{n\sum x_i y_i - \sum x_i \sum y_i}{\sqrt{n\sum x_i^2 - \left(\sum x_i^2\right)}\sqrt{n\sum y_i^2 - \left(\sum y_i^2\right)}} \quad (5)$$

The corner values in the matrix are 1 s for the same two variables. As an example, a large positive correlation was noted from the matrix when r = 1.00 between T_e and T_{ee}. Similarly, one small positive correlation was noted, that is, r = 0.04 between T_e and T_p. A large negative correlation was noted from the matrix when r = −0.84 between V_y and location.

The correlation matrix generation was attempted to understand the different variables affecting the performance probability parameters and the overall efficiency of the UTC before it is accepted for any use such as drying. It was necessary to obtain insight into the behavior of the variables concerning changes in another variable that directly or indirectly affected the performance of UTC.

Table 3. Correlation matrix.

	Location	**T_p**	**V_y**	**T_e**	**T_{pe}**	**T_{ee}**
Location	1.00	0.29	−0.84	−0.12	0.33	−0.16
T_p	0.29	1.00	−0.07	0.04	0.99	0.06
V_y	−0.84	−0.07	1.00	0.35	−0.11	0.37
T_e	−0.12	0.04	0.35	1.00	0.02	1.00
T_{pe}	0.33	0.99	−0.11	0.02	1.00	0.05
T_{ee}	−0.16	0.06	0.37	1.00	0.05	1.00

The correlation matrix establishes a statistical foundation [43] to understand the linear relationship, and it also provides a clue to narrow down the search for ways to focus on those variables that are sensitive to a small change with respect to the causation of another variable. More importantly, these continuous variables are ingredients of the performance prediction. One of the methods to predict the performance probability of the system (in this case, a UTC) is the Monte Carlo simulation. The above-mentioned variables were integral parts of the simulation [44,45].

The Monte Carlo simulation is a mathematical technique (shown in Figure 5f) used to understand the impact of risk and uncertainty in prediction and forecasting models. It is an algorithm that depends upon random numbers (or a random sample of observations or data) to produce the numerical result that is desired from the outcome of the method. Essentially, the concept of the Monte Carlo simulation uses randomness, which can be brought by different distributions of solution space to solve a problem that might be deterministic.

Monte Carlo technique has been used to predict the overall performance of a flat UTC. The performance of the UTC was studied through its thermal efficiency [1], that is

$$\eta = \rho \times V_s \times C_p \times (T_e - T_\infty)/G \quad (6)$$

where the density of air (ρ) is 1.22 kg/m^3, suction velocity (V_s) is kept between 0.045 m/s and 0.077 m/s, the specific heat capacity of air at constant pressure (C_p) is 1.005 kJ/kg·K,

exit temperature (T_e) and freestream temperature (T_∞) are in Kelvin (K), and solar radiation (G) on the UTC is in Watt/m^2.

The simulation was run 1000 times to compute the likelihood (41%) of efficiency that could be acceptable for use. The acceptability of use was decided based on the drying capacity of the UTC. The simulation also predicted the likelihood of T_e going greater than 325 K (close to 52 °C) where drying is possible and affects the system's efficiency [46–48].

The simulation was carried out using the randomness of input variables such as T_e, T_∞ and V_s, and then the efficiency of the UTC was computed for each sample. The efficiency values beyond 35% were accepted for use. So, the variation in system efficiency was between 35% and 65% in this study. The same variation is displayed in the abscissa of Figure 6a–c. In the ordinate of Figure 6a–c is shown the variable that varies with system efficiency.

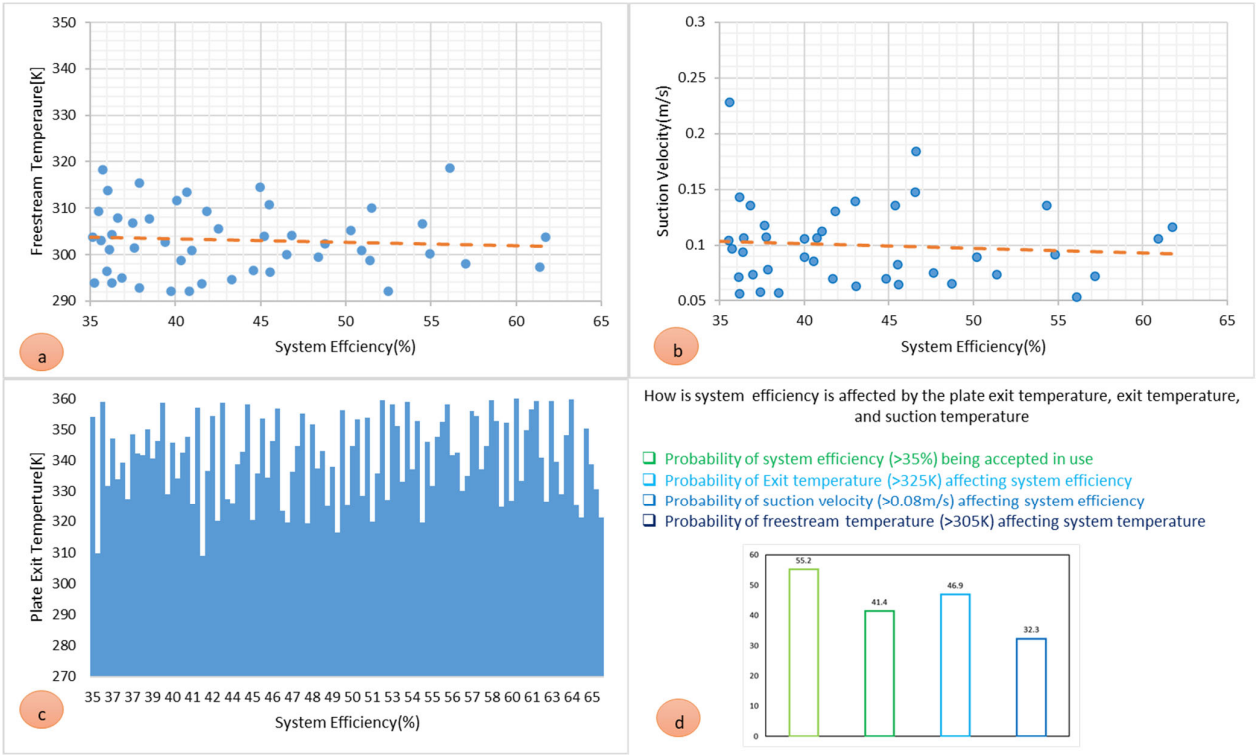

Figure 6. (**a**) Probability of freestream temperature (**b**) Probability of suction velocity (**c**) Probability of plate exit temperature (**d**) Combined Probability graph.

From Figure 6a, it was also noted that the likelihood (or probability) of freestream (T_∞ greater than 305 K) influenced about 32.3% of the system efficiency, and a trend line passing inside the variation of data indicated that the average freestream temperature remained at 300 K during the simulation. From Figure 6b, it was also noted that the likelihood (or probability) of suction velocity (V_s beyond 0.08 m/s) influenced about 46.9% of the system efficiency in this study, and a trend line drawn in the collected data points indicated that the suction velocity remained between 0.05 m/s and 0.1 m/s (in Ref. [1]). V_s was between 0.045 and 0.077 m/s.

From Figure 6c, it was also noted that the probability of plate exit temperature (T_e beyond 325 K) influenced about 41.4% of the system efficiency, and a trend line passing through data shown in the plot indicated that the exit temperature remained at 320 K. So, the difference between the freestream value of temperature and that value inside the chamber varied between 15 and 20 °C. Heated chambers usually can be implemented for drying (the typical range of drying is 10 to 15 °C) purposes. Figure 6d gives the summary of flat UTC performance with an observation that the probability of system efficiency greater

than 35% is 55.2%. This raised the hope of recommending the UTC for drying and heating applications where the required temperature differential is within 20 °C [49–51].

Pair plots are shown in in Figure 7 below. From these plots, the relationship among T_p, T_e, $T_{rise,}$ and the efficiency/maximum efficiency (Eff) ratio in a single plot could be known. It was observed that T_p and T_e were strongly correlated and showed a relationship where both varied linearly. Similarly, T_e and T_{rise} had a strong linear relationship and the Eff ratio had a linear relationship with T_{rise}.

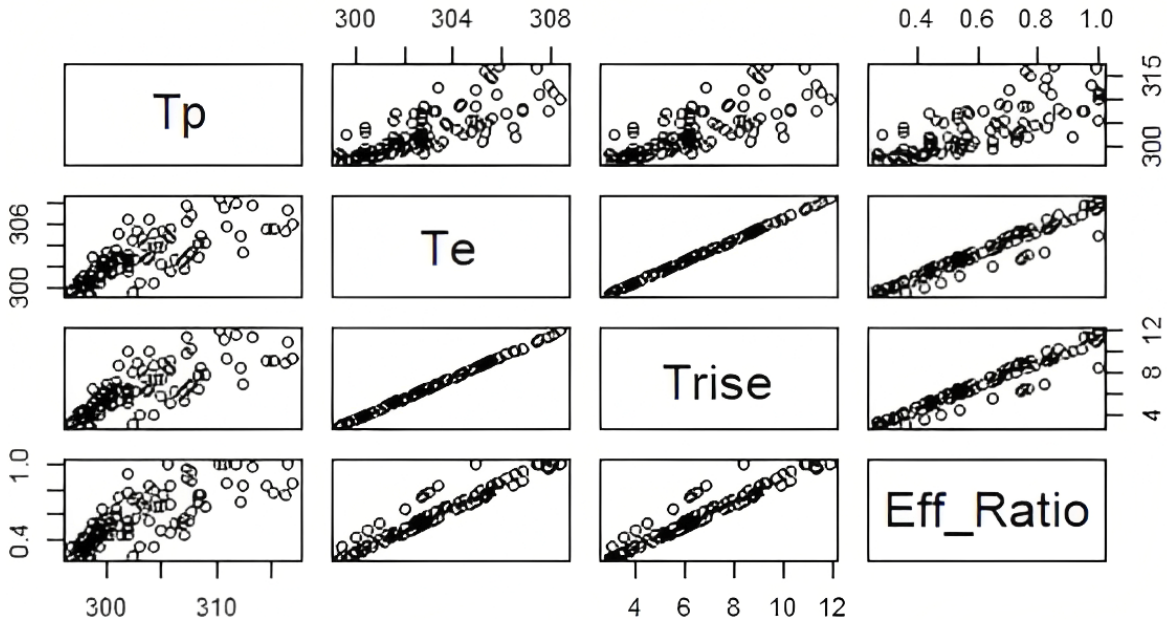

Figure 7. Relationship among T_p, T_e, T_{rise}, and efficiency/maximum efficiency (Eff) ratio in a flat UTC.

Computational methods were adopted to check the performance of the system with key variables. The fitted value (or regression line) for the response variables (as shown in Figures 4d,e and 5a–e) confirmed the presence of outliers (data points far from the regression line) in the actual data, and hence, these were ignored. The study predicted a strong correlation with the cavity vertical velocity, and a weaker correlation was determined for the exit and plate temperatures [52–55].

The Monte Carlo simulation predicted the likelihood of T_e going greater than 325 K (close to 52 °C), and hence, drying with the hot air collected in the cavity (or chamber) could be possible. The simulation also revealed the likelihood of system efficiency being affected by the key decision variables such as suction velocity (V_s), plate exit temperature (T_e), and freestream temperature (T_∞).

4. Conclusions

From the Monte Carlo simulation, the probability of present system efficiency being influenced by key resolving variables such as freestream temperature (T_∞), suction velocity (V_s), and plate exit temperature (T_e) was noted. It was also noted that the probability of freestream temperature (T_∞ greater than 305 K) influences about 32.3% of the system efficiency. The probability of suction velocity (V_s beyond 0.08 m/s) influences about 46.9% of system efficiency, while the probability of plate exit temperature (T_e beyond 325 K) influences about 41.4% of system efficiency. The difference between the freestream value of temperature and the value inside the chamber varied between 15 and 20 °C. Another observation from the study was that the probability of system efficiency of greater than 35% was 55.2%. This has raised the hope of recommending UTCs for drying and heating applications where the required temperature differential is within 20 °C. The

predicted average plate exit temperature remained at 320 K, which was also noted during the experiment. The performance probability prediction for the UTC was a key decision-making factor in the design of UTCs—both the flat and corrugated types.

Author Contributions: Conceptualization, S.P.P. and S.K.M.; methodology, S.P.P.; software, T.R.; validation, S.K.M., S.P.P. and R.G.; formal analysis, S.K.M.; investigation, S.P.P.; writing—original draft preparation, M.H.A.; writing—review and editing, C.A.S. and M.S.; visualization, T.R.; supervision, M.A.; funding acquisition, M.A. All authors have read and agreed to the published version of the manuscript.

Funding: This research received no external funding.

Acknowledgments: The authors extend their appreciation to the Deanship of Scientific Research at King Khalid University, Saudi Arabia, for funding this work through Research Group Program under Grant No. R.G.P. 1/256/43.

Conflicts of Interest: The authors declare no conflict of interest.

References

1. Li, S.; Karava, P. Evaluation of turbulence models for airflow and heat transfer prediction in BIPV/T systems optimization. *Energy Procedia* **2012**, *30*, 1025–1034. [CrossRef]
2. Li, S.; Karava, P.; Currie, S.; Lin, W.E.; Savory, E. Energy modeling of photovoltaic thermal systems with corrugated unglazed transpired solar collectors—Part 2: Performance analysis. *Sol. Energy* **2014**, *102*, 297–307. [CrossRef]
3. Li, S.; Karava, P.; Savory, E.; Lin, W.E. Airflow and thermal analysis of flat and corrugated unglazed transpired solar collectors. *Sol. Energy* **2013**, *91*, 297–315. [CrossRef]
4. Li, S.; Karava, P.; Currie, S.; Lin, W.E.; Savory, E. Energy modeling of photovoltaic thermal systems with corrugated unglazed transpired solar collectors—Part 1: Model development and validation. *Sol. Energy* **2014**, *102*, 282–296. [CrossRef]
5. Croitoru, C.V.; Nastase, I.; Bode, F.I.; Meslem, A. Thermodynamic investigation on an innovative unglazed transpired solar collector. *Sol. Energy* **2016**, *131*, 21–29. [CrossRef]
6. Vaziri, R.; Ilkan, M.; Egelioglu, F. Experimental performance of perforated glazed solar air heaters and unglazed transpired solar air heater. *Sol. Energy* **2015**, *119*, 251–260. [CrossRef]
7. Collins, M.R.; Abulkhair, H. An evaluation of heat transfer and effectiveness for unglazed transpired solar air heaters. *Sol. Energy* **2014**, *99*, 231–245. [CrossRef]
8. Badache, M.; Rousse, D.R.; Hallé, S.; Quesada, G.; Quesada, G. Experimental and numerical simulation of a two-dimensional unglazed transpired solar air collector. *Sol. Energy* **2013**, *93*, 209–219. [CrossRef]
9. Arulanandam, S.J.; Hollands, K.G.T.; Brundrett, E. A CFD heat transfer analysis of the transpired solar collector under no-wind condition. *Sol. Energy* **1999**, *67*, 93–100. [CrossRef]
10. Panigrahi, S.P.; Maharan, S.K. Correlation of temperature, velocity and perforation location in a flat unglazed transpired solar collector (Utc) due to air flow. *JP J. Heat Mass Trans.* **2020**, *19*, 1–18. [CrossRef]
11. Gawlik, K.M. A Numerical and Experimental Investigation of Heat Transfer Issues in the Practical Utilization of Unglazed, Transpired Solar Air Heaters. Ph.D. Thesis, University of Colorado, Boulder, CO, USA, 1993.
12. Gawlik, K.M.; Kutscher, C.F. Wind Heat Loss from Corrugated, Transpired Solar Collectors. *J. Sol. Energy Eng.* **2002**, *124*, 256–261. [CrossRef]
13. Iglisch, R. *Exact Calculation of Laminar Boundary Layer in Longitudinal Flow over a Flat Plate with Homogeneous Suction*; Schriften der Deutschen Akademie der Luftfahrtforschung, Band 8B, Heft 1; NACA: Boston, MA, USA, 1994; Translation: NACA TM No. 1205.
14. Kutscher, C.; Christensen, C.; Barker, G. Unglazed Transpired Solar Collectors—An Analytical Model and Test-Results. In *1991 Solar World Congress*; Arden, M.E., Burley, S.M.A., Coleman, M., Eds.; Elsevier: Amsterdam, The Netherlands, 1992; Volume 2, pp. 1245–1250.
15. Motahar, S.; Alemrajabi, A.A. An analysis of unglazed transpired solar collectors based on exergetic performance criteria. *Int. J. Thermodyn.* **2010**, *13*, 153–160.
16. Shukla, A.; Nkwetta, D.N.; Cho, Y.J.; Stevenson, V.; Jones, P. A state of art review on the transpired solar collector. *Renew. Sustain. Energy Rev.* **2012**, *16*, 3975–3985. [CrossRef]
17. Kutscher, C.F.; Christensen, C.; Barker, G. Unglazed transpired solar collectors: An analytic model and test results. In Proceedings of the ISES Solar World Congress, Denver, CO, USA, 19–23 August 1991; Elsevier Science: Amsterdam, The Netherlands, 1991; pp. 1245–1250.
18. Athienitis, A.K.; Bambara, J.; O'Neill, B.; Faille, J. A prototype photovoltaic/thermal system integrated with transpired collector. *Sol. Energy* **2011**, *85*, 139–153. [CrossRef]
19. Dymon, C.; Kutscher, C. Development of a flow distribution and design model for transpired solar collectors. *Sol. Energy* **1997**, *60*, 291–300. [CrossRef]

20. Wang, Y.; Shukla, A.; Liu, S. A state of art review on methodologies for heat transfer and energy flow characteristics of the active building envelopes. *Renew. Sustain. Energy Rev.* **2017**, *78*, 1102–1116. [CrossRef]
21. Skoplaki, E.; Palyvos, J.A. On the temperature dependence of photovoltaic module electrical performance: A review of efficiency/power correlations. *Sol. Energy* **2009**, *83*, 614–624. [CrossRef]
22. Cho, Y.J.; Shukla, A.; Nkwetta, D.N.; Jones, P. Thermal modelling and parametric study of transpired solar collector. In *CIBSE ASHRAE Technical Symposium*; Imperial College London: London, UK, 2012; pp. 18–19.
23. Rajashekaraiah, T.; Mura, M.J.; Sharasthantra, R.; Sharma, G.S. Optimizing the efficiency of solar flat plate collector with trapezoidal reflector. *AIP Conf. Proc.* **2019**, *2080*, 030008.
24. Zhang, T.; Tan, Y.; Yang, H.; Zhang, X. The application of air layers in building envelopes: A review. *Appl. Energy* **2016**, *165*, 707–734. [CrossRef]
25. Colangelo, G.; Favale, E.; Miglietta, P.; de Risi, A. Innovation in flat solar thermal collectors: A review of the last ten years experimental results. *Renew. Sustain. Energy Rev.* **2016**, *57*, 1141–1159. [CrossRef]
26. El-Khawajah, M.F.; Aldabbagh, L.B.Y.; Egelioglu, F. The effect of using transverse fins on a double pass flow solar air heater using wire mesh as an absorber. *Sol. Energy* **2011**, *85*, 1479–1487. [CrossRef]
27. Van Decker, G.W.E.; Hollands, K.G.T.; Brunger, A.P. Heat-exchange relations for unglazed transpired solar collectors with circular holes on a square or triangular pitch. *Sol. Energy* **2001**, *71*, 33–45. [CrossRef]
28. Tajdaran, S.; Bonatesta, F.; Ogden, R.; Kendrick, C. CFD modelling of transpired solar collectors and characterisation of multi-scale airflow and heat transfer mechanisms. *Sol. Energy* **2016**, *131*, 149–164. [CrossRef]
29. Li, S.W.; Joe, J.; Hu, J.J.; Karava, P. System identification and model-predictive control of office buildings with integrated photovoltaic-thermal collectors, radiant floor heating and active thermal storage. *Sol. Energy* **2015**, *113*, 139–157. [CrossRef]
30. Semenou, T.; Rousse, D.R.; Le Lostec, B.; Nouanegue, H.F.; Paradis, P.L. Mathematical modelling of dual intake transparent transpired solar collector. *Math. Probl. Eng.* **2015**, *2015*, 942854. [CrossRef]
31. Leon, M.A.; Kumar, S. Mathematical modelling and thermal performance analysis of unglazed transpired solar collectors. *Sol. Energy* **2007**, *81*, 62–75. [CrossRef]
32. Esen, H.; Esen, M.; Ozsolak, O. Modelling and experimental performance analysis of solar-assisted ground source heat pump system. *J. Exp. Theor. Artif. Intell.* **2017**, *29*, 1–17. [CrossRef]
33. Thejaraju, R.; Girisha, K.B.; Manjunath, S.H.; Dayananda, B.S. Numerical evaluation of thermo-hydraulic performance index of a double pipe heat exchanger using double sided louvered winglet tape. *J. Therm. Eng.* **2020**, *6*, 843–857. [CrossRef]
34. Belusko, M.; Saman, W.; Bruno, F. Roof integrated solar heating system with glazed collector. *Sol. Energy* **2004**, *76*, 61–69. [CrossRef]
35. Rounisa, E.D.; Bigaila, E.; Luka, P.; Athienitis, A.; Stathopoulos, T. Multiple-inlet BIPV/T modeling: Wind effects and fan induced suction. *Energy Procedia* **2015**, *78*, 1950–1955. [CrossRef]
36. Belusko, M. Investigation into a Roof Integrated Solar Space Air Heater. Honours Master's Thesis, University of South Australia, Adelaide, Australia, 1996.
37. Greig, D.; Siddiqui, K.; Karava, P. An experimental investigation of the flow structure over a corrugated waveform in a transpired air collector. *Int. J. Heat Fluid Flow* **2012**, *38*, 133–144. [CrossRef]
38. Badache, M.; Halle, S.; Rousse, D.R.; Quesada, G.; Dutil, Y. An experimental investigation of a two-dimensional prototype of a transparent transpired collector. *Energy Build.* **2014**, *68*, 232–241. [CrossRef]
39. Ozgen, F.; Esen, M.; Esen, H. Experimental investigation of thermal performance of a double-flow solar air heater having aluminum cans. *Renew. Energy* **2009**, *11*, 2391–2398. [CrossRef]
40. Bejan, A.S.; Teodosiu, C.; Croitoru, C.V.; Catalina, T.; Nastase, I. Experimental investigation of transpired solar collectors with/without phase change materials. *Sol. Energy* **2021**, *214*, 478–490. [CrossRef]
41. Bejan, A.-S.; Croitoru, C.; Bode, F.; Teodosiu, C.; Catalina, T. Experimental investigation of an enhanced transpired air solar collector with embodied phase changing materials. *J. Clean. Prod.* **2022**, *336*, 130398. [CrossRef]
42. *Ansys Fluent Theory Guide*; Release 2022 R2; Ansys Inc.: Canonsburg, PA, USA, 2022; p. 15317.
43. Freedman, D.; Pisani, R.; Purves, R. *Statistics (International Student Edition)*, 4th ed.; Pisani, R., Purves, R., Eds.; WW Norton & Company: New York, NY, USA, 2007.
44. Saleh, B.; Sundar, L.S.; Aly, A.A.; Ramana, E.V.; Sharma, K.V.; Afzal, A.; Abdelrhman, Y.; Sousa, A.C.M. The Combined Effect of Al_2O_3 Nanofluid and Coiled Wire Inserts in a Flat-Plate Solar Collector on Heat Transfer, Thermal Efficiency and Environmental CO_2 Characteristics. *Arab. J. Sci. Eng.* **2022**, *47*, 9187–9214. [CrossRef]
45. Felemban, B.F.; Essa, F.A.; Afzal, A.; Ahmed, M.H.; Saleh, B.; Panchal, H.; Shanmugan, S.; Elsheikh, A.; Omara, Z.M. Experimental Investigation on Dish Solar Distiller with Modified Absorber and Phase Change Material under Various Operating Conditions. *Environ. Sci. Pollut. Res.* **2022**, *29*, 63248–63259. [CrossRef]
46. Kumar, R.; Nadda, R.; Kumar, S.; Razak, A.; Sharifpur, M.; Aybar, H.S.; Ahamed Saleel, C.; Afzal, A. Influence of Artificial Roughness Parametric Variation on Thermal Performance of Solar Thermal Collector: An Experimental Study, Response Surface Analysis and ANN Modelling. *Sustain. Energy Technol. Assess.* **2022**, *52*, 102047. [CrossRef]
47. Attia, M.E.H.; Thalib, M.M.; Kumar, S.; Afzal, A.; Vaithilingam, S.; Sathyamurthy, R.; Manokar, A.M. Water Quality Analysis of Solar Still Distillate Produced from Various Water Sources of El Oued Region Algeria. Desalin. *Water Treat.* **2022**, *253*, 55–62. [CrossRef]

48. Santhosh Kumar, P.C.; Naveenkumar, R.; Sharifpur, M.; Issakhov, A.; Ravichandran, M.; Mohanavel, V.; Aslfattahi, N.; Afzal, A. Experimental Investigations to Improve the Electrical Efficiency of Photovoltaic Modules Using Different Convection Mode. *Sustain. Energy Technol. Assess.* **2021**, *48*, 101582. [CrossRef]
49. Benoudina, B.; Attia, M.E.H.; Driss, Z.; Afzal, A.; Manokar, A.M.; Sathyamurthy, R. Enhancing the Solar Still Output Using Micro/Nano-Particles of Aluminum Oxide at Different Concentrations: An Experimental Study, Energy, Exergy and Economic Analysis. *Sustain. Mater. Technol.* **2021**, *29*, e00291. [CrossRef]
50. Samylingam, L.; Aslfattahi, N.; Saidur, R.; Mohd, S.; Afzal, A. Solar Energy Materials and Solar Cells Thermal and Energy Performance Improvement of Hybrid PV/T System by Using Olein Palm Oil with MXene as a New Class of Heat Transfer Fluid. *Sol. Energy Mater. Sol. Cells* **2020**, *218*, 110754. [CrossRef]
51. Samuel, O.D.; Kaveh, M.; Oyejide, O.J.; Elumalai, P.V.; Verma, T.N.; Nisar, K.S.; Saleel, C.A.; Afzal, A.; Fayomi, O.S.I.; Owamah, H.I.; et al. Performance Comparison of Empirical Model and Particle Swarm Optimization & Its Boiling Point Prediction Models for Waste Sunflower Oil Biodiesel. *Case Stud. Therm. Eng.* **2022**, *33*, 101947. [CrossRef]
52. Kumar, R.; Nadda, R.; Kumar, S.; Kumar, K.; Afzal, A.; Razak, K.A.; Sharifpur, M. Heat Transfer and Friction Factor Correlations for an Impinging Air Jets Solar Thermal Collector with Arc Ribs on an Absorber Plate. *Sustain. Energy Technol. Assess.* **2021**, *47*, 101523. [CrossRef]
53. Akram, N.; Montazer, E.; Kazi, S.N.; Soudagar, M.E.M.; Ahmed, W.; Zubir, M.N.M.; Afzal, A.; Muhammad, M.R.; Ali, H.M.; Márquez, F.P.G.; et al. Experimental Investigations of the Performance of a Flat-Plate Solar Collector Using Carbon and Metal Oxides Based Nanofluids. *Energy* **2021**, *227*, 120452. [CrossRef]
54. Zare, S.; Ayati, M.; Ha'iriYazdi, M.R.; Kabir, A.A. Convolutional neural networks for wind turbine gearbox health monitoring. *Energy Equip. Syst.* **2022**, *10*, 73–82.
55. Sabzi, S.; Asadi, M.; Moghbelli, H. Review, analysis and simulation of different structures for hybrid electrical energy storages. *Energy Equip. Syst.* **2017**, *5*, 115–129.